Springer手册精选系列

电子与光子材料手册

电子材料

【第3册】

Springer Handbook of

Electronic and Photonic Materials

Kasap
r Capper 主编

（影印版）

哈尔滨工业大学出版社
HARBIN INSTITUTE OF TECHNOLOGY PRESS

Springer Handbook of Electronic and Photonic Materials

Safa Kasap, Peter Capper (Eds.)

Springer

黑版贸审字08-2012-031号

图书在版编目（CIP）数据

电子与光子材料手册. 第3册，电子材料=Handbook of Electronic and Photonic Materials Ⅲ Materials for Electronics：英文／（加）卡萨普（Kasap S.），（英）卡珀（Capper P.）主编. —影印本. —哈尔滨：哈尔滨工业大学出版社，2013.1

（Springer手册精选系列）

ISBN 978-7-5603-3762-3

Ⅰ. ①电… Ⅱ. ①卡…②卡… Ⅲ. ①电子材料-手册-英文②光学材料-手册-英文Ⅳ. ①TN04-62②TB34-62

中国版本图书馆CIP数据核字（2012）第190658号

材料科学与工程
图书工作室

责任编辑 杨 桦 张秀华
出版发行 哈尔滨工业大学出版社
社 址 哈尔滨市南岗区复华四道街10号 邮编 150006
传 真 0451-86414749
网 址 http://hitpress.hit.edu.cn
印 刷 哈尔滨市石桥印务有限公司
开 本 787mm × 960mm 1/16 印张 20.5
版 次 2013年1月第1版 2013年1月第1次印刷
书 号 ISBN 978-7-5603-3762-3
定 价 58.00元

目 录

Contents

Part C Materials

Part C Materials for Electronics

21. Single-Crystal Silicon: Electrical and Optical Properties

Electrical and optical properties of crystalline semiconductors are important parts of pure physics and material science research. In addition, knowledge of parameters related to these properties, primarily for silicon and III–V semiconductors, has received a high priority in microelectronics and optoelectronics since the establishment of these industries. For control protocols, emphasis has recently been placed on novel optical measurement techniques, which have proved very promising as nondestructive and even non-contact methods. Earlier they required knowledge of the free-carrier-derived optical constants, related to the electrical conductivity at infrared frequencies, but interest in the optical constants of silicon in the visible, ultraviolet (UV) and soft-X-ray ranges has been revived since the critical dimensions in devices have become smaller.

This chapter surveys the electrical (Sect. 21.2) and optical (Sect. 21.3) properties of crystalline silicon. Section 21.2 overviews the basic concepts. Though this section is bulky and its material is documented in textbooks, it seems worth including since the consideration here focuses primarily on silicon and is not spread over other semiconductors – this makes the present review self-contained. To avoid repeated citations we, in advance, refer the reader to stable courses on solid-state physics (e.g. [21.1, 2]), semiconductor physics (e.g. [21.3]), semiconductor optics (e.g. [21.4]) and electronic devices (e.g. [21.5]); seminal papers are cited throughout Sect. 21.2.

We realize how formidable our task is – publications on electrical and optical properties of silicon amount to a huge number of titles, most dating back to the 1980s and 1990s – so any review of this subject will inevitably be incomplete. Nevertheless, we hope that our work will serve as a useful shortcut into the silicon world for a wide audience of applied physics, electrical and optical engineering students.

21.1 Silicon Basics

21.1.1 Structure and Energy Bands

Normally silicon (Si) crystallizes in a diamond structure on a face-centered cubic (f.c.c.) lattice, with a lattice constant of $a_0 = 5.43$ Å. The basis of the diamond structure consists of two atoms with coordinates (0, 0, 0) and $a_0/4(1, 1, 1)$, as seen in Fig. 21.1. Other solids that can crystallize in the diamond structure are C, Ge and Sn. The important notion for the electronic band structure is the Brillouin zone (BZ). The BZ is a primitive cell in the reciprocal-space lattice, which proves to be a body-centered cubic (b.c.c.) lattice for an f.c.c. real-space lattice. For this case, the BZ with important reference points and directions within it is shown in Fig. 21.2.

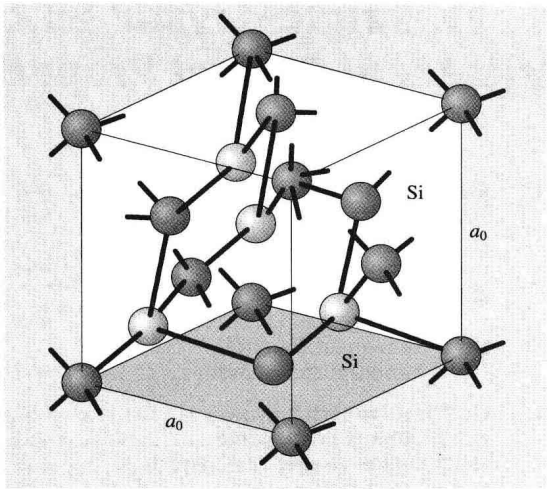

Fig. 21.1 Diamond crystal structure of Si

The states of electrons in solids are described by wave functions of the Bloch type

$$\psi(\boldsymbol{r}) = \mathrm{e}^{\mathrm{i}\boldsymbol{k}\cdot\boldsymbol{r}} u_{s\boldsymbol{k}}(\boldsymbol{r}) \,, \tag{21.1}$$

where $\boldsymbol{k}$ is the wave vector that runs over reciprocal space, s is a band index and $u_{s\boldsymbol{k}}(\boldsymbol{r})$ is the periodic function of the direct lattice (Bloch amplitude). Both $u_{s\boldsymbol{k}}(\boldsymbol{r})$ and the corresponding energy-band spectrum $E_s(\boldsymbol{k})$ are periodic in $\boldsymbol{k}$, which allows one to restrict consideration

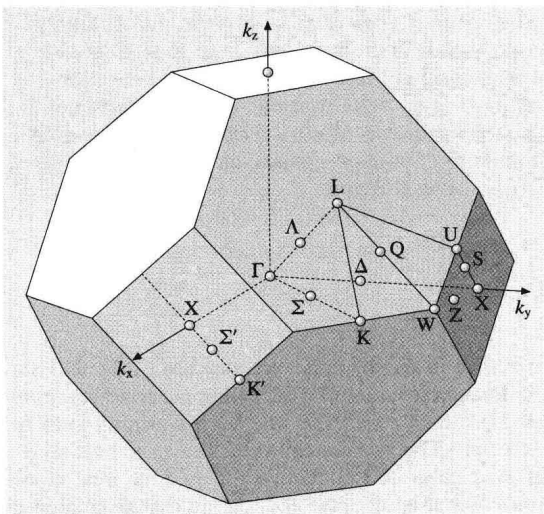

Fig. 21.2 Brillouin zone of the f.c.c. lattice

to within the BZ. The bands are arranged so that there are energy regions for which no states given by (21.1) exist. Such forbidden regions are called energy gaps or band gaps and result from the interaction of valence electron with the ion cores of crystal. In semiconductor science the term *band gap* is accepted for the energy distance between the maximum of $E_s(\boldsymbol{k})$ for the highest filled (valence) band and the minimum of $E_s(\boldsymbol{k})$ for the lowest empty (conduction) band (denoted by E_g). The band gap is called *direct* if the aforementioned maximum and minimum occur at the same point of the BZ, e.g. Γ (Fig. 21.2), and *indirect* if they occur at different points of the BZ, e.g. Γ and X (Fig. 21.2).

Si is an indirect-band-gap semiconductor with $E_g = 1.1700\,\mathrm{eV}$ at 4.2 K. The calculated energy-band structure, that is the curves of $E_v(\boldsymbol{k})$ for selected directions in the BZ, is shown in Fig. 21.3a. The conduction-band minimum lies at six equivalent points Δ on the Γ–X lines (Fig. 21.2). In some vicinity (called the *valley*) of every such point the band spectrum is quadratic in $\boldsymbol{k}$, e.g. for the valley $\langle 100\rangle$

$$E_c(\boldsymbol{k}) = E_{c0} + \frac{\hbar^2 (k_x - k_0)^2}{2m_\mathrm{l}} + \frac{\hbar^2 \left(k_y^2 + k_z^2\right)}{2m_\mathrm{t}} \,, \tag{21.2}$$

where $k_0 \approx 1.72\pi/a_0$, m_l and m_t are the longitudinal and transverse effective masses. The spectra for other five valleys are obtained from (21.2) by 90° rotations and inversions $k_0 \to -k_0$. Though the constant-energy surface for (21.2) is an ellipsoid (Fig. 21.3b), the density of states (DOS) proves to be the same as for an isotropic parabolic spectrum with an effective mass

$$m_{de} = 6^{2/3} m_\mathrm{l}^{1/3} m_\mathrm{t}^{2/3} \,, \tag{21.3}$$

which is called the *DOS effective mass*. Another mass, m_{ce}, which appears in the direct-current (DC) and optical conductivity formulas, is defined via the harmonic mean

$$\frac{1}{m_{ce}} = \frac{1}{3}\left(\frac{1}{m_\mathrm{l}} + \frac{2}{m_\mathrm{t}}\right) \,. \tag{21.4}$$

For this reason, m_c is called the *conductivity/optical effective mass*. Equation (21.2) holds at $E_c - E_{c0} < 0.15\,\mathrm{eV}$, but at larger energies the ellipsoids warp strongly, especially near the X point; the change of the spectrum with energy is mostly due to the increasing m_t, while m_l increases weakly [21.6].

The valence-band maximum is at the Γ point ($\boldsymbol{k} = 0$), where the Bloch-wave state $u_{n0}(\boldsymbol{r})$ has the full symmetry of an atomic p-orbital, being six-fold degenerate in the nonrelativistic limit. The spin–orbit interaction splits

off from the bare band top a four-fold degenerate $p_{3/2}$ level up by $1/3\Delta_{so}$, and a two-fold degenerate $p_{1/2}$ level down by $-2/3\Delta_{so}$. The spectrum at $\boldsymbol{k} \neq 0$, even at energies near the top E_{v0}, is very complex. It consists of three branches, which are in general nonparabolic and nonisotropic [21.7]. At $E_{v0} - E_v \ll \Delta_{so}$ there are two nonparabolic anisotropic $p_{3/2}$-derived sub-bands with the energy spectra

$$E_{v1,2}(\boldsymbol{k}) = E_{v0} + \frac{\hbar^2}{2m_0}\left[Ak^2 \pm \sqrt{B^2k^4 + C^2\left(k_x^2k_y^2 + k_x^2k_z^2 + k_y^2k_z^2\right)}\right], \quad A < 0 \tag{21.5}$$

and at $E_{v0} - E_v \ll 2\Delta_{so}$ these is an isotropic parabolic $p_{1/2}$-derived split-off band with the energy spectrum

$$E_{v3}(\boldsymbol{k}) = E_{v0} - \Delta_{so} + \frac{\hbar^2k^2}{2m_0}A', \quad A' < 0. \tag{21.6}$$

Here m_0 is the free electron mass, A, B, C and A' are inverse hole-mass parameters (for small Δ_{so}, $A' \approx A$). In (21.5) the + sign corresponds to heavy holes and the − sign to light holes. The constant-energy surfaces for (21.5) are warped spheres (Fig. 21.3c), the DOS is nevertheless parabolic and is described by the effective mass

$$m_{dh} = \left(m_{d1}^{3/2} + m_{d2}^{3/2}\right)^{2/3}, \tag{21.7}$$

where $m_{d1,2}$ are the partial DOS effective masses. Quite different masses enter various physical quantities for heavy (light) holes, and are complicated functions of A, B and C ([21.9]); however, the split-off band is characterized by only one effective mass: $m_3 = m_0/|A'|$.

These band-structure parameters, obtained from cyclotron-resonance data and calculations, are presented in Tables 21.2 and 21.3. The unreferenced values of m_{de}, m_{ce} and m_3 were calculated from the referenced data using (21.3, 4) and the assumption $A' = A$. Optical data for m_{ce} are discussed in Sect. 21.3, while the specific-heat data for m_{de} are not considered here.

Considerable uncertainty and errors in the values of B and C have a small effect on the light-hole effective-mass values (m_{d2} and optical m_{c2}) but lead to an ambiguity in the heavy-hole effective-mass (m_{d1} and optical m_{c1}) values (Table 21.3). In each data set $m_{d2} \approx m_{c2}$, which means that an isotropic approximation is reasonable for the light-hole spectrum.

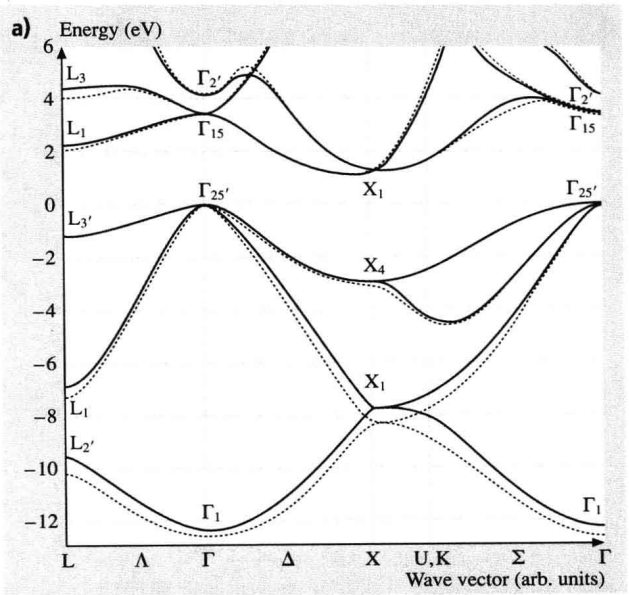

Fig. 21.3 Electronic band structure of Si:(**a**) Energy dispersion curves near the fundamental gap. After [21.8] with permission;

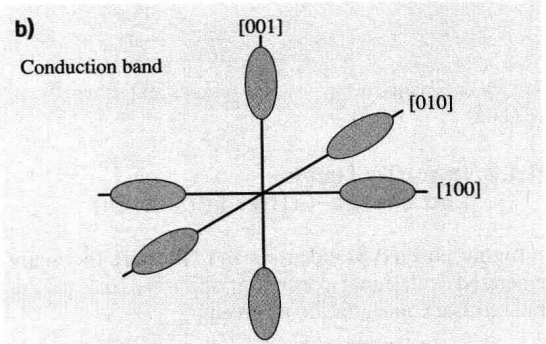

Fig. 21.3 (**b**) The constant-energy ellipsoids of the conduction band;

The experimental data [21.10, 11] and band-structure calculations [21.12] are in good agreement; the former is used in theoretical papers on hole transport in Si [21.13, 14].

Nonparabolic parts in the electron [21.6] and hole spectra [21.7] lead to apparent dependence of effective-mass measurements on the temperature and carrier concentration [21.15]. Recently the DOS mass issue was revisited [21.16] in connection with the intrinsic carrier concentration.

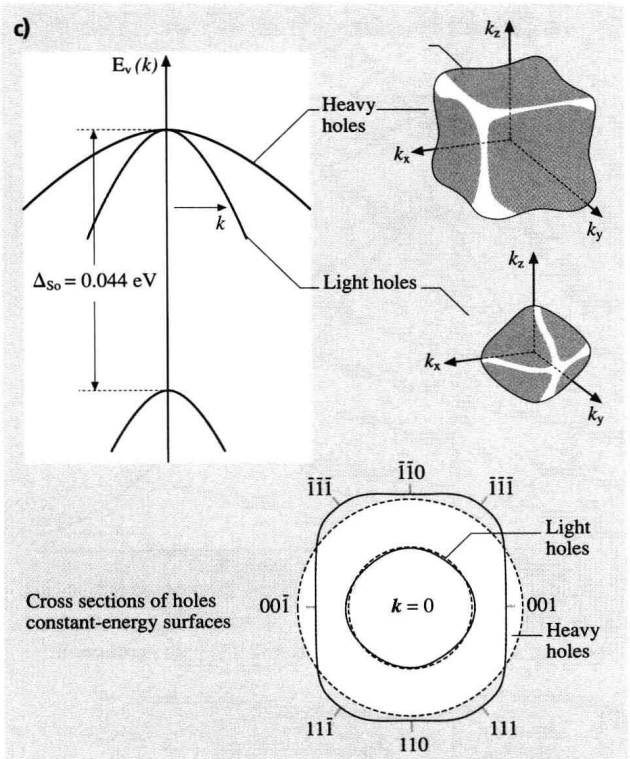

Fig. 21.3 (c) The constant-energy warped spheres and schematic of the valence band

21.1.2 Impurity Levels and Charge-Carrier Population

In highly purified Si electrons and holes are thermally generated with equal concentrations ($n = p$), equal to the intrinsic concentration n_i given by

$$n_i = 2\left(\frac{2\pi\sqrt{m_{de}m_{dh}}k_BT}{h^2}\right)^{3/2}\exp\left(-\frac{E_g}{2k_BT}\right), \quad (21.8)$$

where k_B and h are the Boltzmann and Planck constants, respectively, and T is the absolute temperature. To assess $n_i(T)$ theoretically one should take into account possible changes of $m_{de,h}$ and E_g with T. An early experimental plot of $n_i(T)$ for Si is shown in Fig. 21.4, giving $n_i(300\,\mathrm{K}) = 1.38\times10^{10}\,\mathrm{cm}^{-3}$. This and the early textbook value ($1.45\times10^{10}\,\mathrm{cm}^{-3}$) do not fit (21.8) with the established low-temperature values of $m_{de,h}$ and $E_g(300\,\mathrm{K}) = 1.1242\,\mathrm{eV}$, giving $(0.662–0.694)\times10^{10}\,\mathrm{cm}^{-3}$ for the best available data.

This discrepancy was eliminated [21.16] by critically evaluating measurements of $n_i(T)$ and incorporating the latest data for the hole DOS effective mass. The reassessed value of n_i (300 K), verified by measurements on solar-cell devices [21.17], is $1.08(8)\times10^{10}\,\mathrm{cm}^{-3}$ (in a very recent textbook [21.18] the unreferenced value $n_i(300\,\mathrm{K}) = 1.00\times10^{10}\,\mathrm{cm}^{-3}$ is adopted). This is obtained from (21.8) using $m_{de}(300\,\mathrm{K}) = 1.08m_0$, which is quite close to the tabular values presented, and $m_{dh}(300\,\mathrm{K}) = 1.15m_0$, which is 1.8–2.1 times larger than the tabular values presented. Such a strong increase of m_{dh} when increasing T from 4.2 to 300 K is anticipated from the nonparabolic part of the hole spectra [21.7].

In impure samples $n \neq p$; the charge-neutrality condition is then

$$n - N_d^+ = p - N_a^- \quad (21.9)$$

together with the known expressions for n, p (with $np = n_i^2$ holding until the carriers become degenerate) and the concentrations of charged donors N_d^+ and acceptors N_a^- via the Fermi energy E_F and impurity ionization energies

Table 21.1 Energy levels of impurities in Si

Impurity	Donor/ acceptor	Below conduction band (eV)	Above conduction band (eV)
Ag	D	0.310	
	A		0.210
Al	A		0.057
As	D	0.049	
Au	D		0.330
	A	0.540	
B	A		0.045
Cu	A		0.490
	D		0.240
Fe	D	0.550	
	D		0.400
Ga	A		0.065
In	A		0.160
Li	D	0.033	
Mn	D	0.530	
P	D	0.044	
Sb	D	0.039	
S	D	0.180	
	D	0.370	
Zn	A	0.550	
	A		0.300

Table 21.2 The conduction-band effective masses and valence-band parameters for Si

Conduction band				
Mass	m_l/m_0	m_t/m_0	m_{de}/m_0	m_{ce}/m_0
Experiment	0.97 ± 0.04[a]	0.19 ± 0.01[a]	1.08 ± 0.05	0.26 ± 0.01
	0.9163 ± 0.04[b]	0.1905 ± 0.0001[b]	1.0618 ± 0.0005	0.2588 ± 0.0001
Theory	0.971[c]	0.205[c]	1.137	0.2652
	0.9716[d]	0.1945[d]	1.0978	0.2780

Valence band					
Parameter	Δ_{so}	A	$\lvert B\rvert$ or B	$\lvert C\rvert$	m_3/m_0
Experiment	0.0441 ± 0.004[g]	-4.1 ± 0.2[a]	1.6 ± 0.2[a]	3.3 ± 0.2[a]	0.24 ± 0.01
		-4.28 ± 0.02[e]	-0.75 ± 0.04[e]	5.25 ± 0.05[e]	0.234 ± 0.001
		-4.27 ± 0.02[h]	-0.63 ± 0.08[h]	4.93 ± 0.15[h]	0.234 ± 0.001
Theory		−4.38[c]	0.84[c]	4.11[c]	0.23
	0.04[d]	−4.38[d]	−1.00[d]	4.80[d]	0.23
	0.044[f]	−4.22[f]	−0.78[f]	4.80[f]	0.24

[a] [21.19], [b] [21.20], [c] [21.21], [d] [21.22], [e] [21.10], [f] [21.12], [g] [21.23], [h] [21.11]

Table 21.3 The valence-band effective masses calculated using experimental data

Mass	m_{d1}/m_0	m_{d2}/m_0	m_d/m_0	m_{c1}/m_0	m_{c2}/m_0
Exp.[a]	0.55 ± 0.12	0.16 ± 0.01	0.61 ± 0.12	0.51 ± 0.10	0.16 ± 0.01
Exp.[b]	0.58 ± 0.02	0.151 ± 0.001	0.63 ± 0.02	0.43 ± 0.01	0.145 ± 0.001
Exp.[c]	0.49–0.56	0.153–0.158	0.54–0.62	0.40–0.43	0.147–0.152

[a] [21.19], [b] [21.10], [c][21.11]

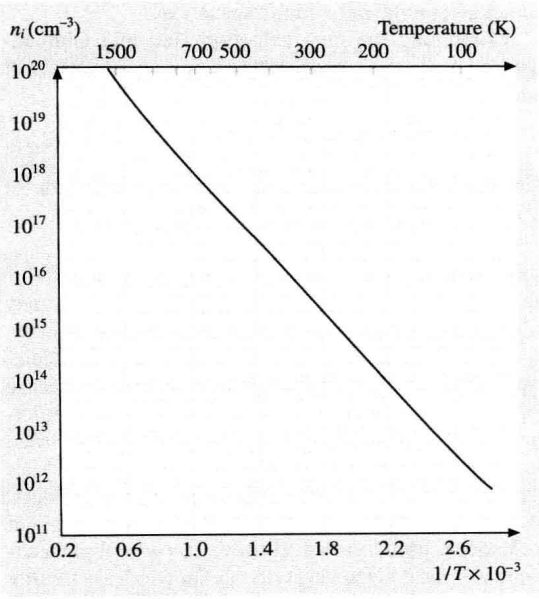

Fig. 21.4 Intrinsic concentration in Si versus temperature. After [21.24] with permission

E_d and E_a allows one to calculate E_F (and hence all the concentrations) as a function of T and doping.

An impurity is called *shallow* if $|E_{c(v)0} - E_{d(a)}| \ll E_g$, and *deep* if $|E_{c(v)0} - E_{d(a)}| \approx 0.5E_g$. Shallow group V donors (Sb, P, As) and group III acceptors (B, Al, Ga, In) are well soluble in Si [21.25]. The ionization energy was calculated using the effective-mass approximation, and the Bohr model for donors [21.26–28] (Kohn and Luttinger, 1955; Kohn, 1955) and acceptors (Luttinger and Kohn, 1955). The value of $E_{d(a)}$ calculated in this way is insensitive to the specific shallow donor (acceptor). Actual thermal (i.e. retrieved from electrical measurements) ionization energies are given in Table 21.1. It is seen that shallow impurities have different ionization energies. This difference is small for donors and larger for acceptors. The same trend was observed for optical ionization energies, although they are different from the thermal values [21.29,30]. For shallow impurities, $E_{d(a)}$ decreases as doping becomes heavier, and becomes zero as $N_{d(a)}$ approaches the corresponding insulator–metal transition concentration [21.31].

Deep impurities (except for Mn, Fe and Zn) are amphoteric, i.e. they act simultaneously as donors and acceptors. For such a donor (acceptor) state, the level

may lie closer to the valence (conduction) than the conduction (valence) band. The deep impurities are mostly unionized at room temperature due to their large $E_{d(a)}$, so their direct contribution to n or p is negligible. The unionized deep impurities may, however, trap the carriers available from the shallow impurities or injection, thus decreasing the conductivity or the minority-carrier lifetime. Atoms that behave in Si in this manner, for example Au, Ag and Cu, are added for lifetime control. The properties of these impurities in Si have been studied in detail (see, e.g., [21.32, 33]).

21.1.3 Carrier Concentration, Electrical and Optical Properties

Concentration and Electrical Measurements

Measurements of carrier concentrations, as well as electrical and optical characteristics are most tractable if either $n \gg p$ (strongly n-type conduction) or $p \gg n$ (strongly p-type conduction). Since the np product is constant versus doping, the contribution of minority carriers to the conductivity becomes unimportant when $N_{d(a)}$ increases significantly over n_i. A standard route for determining $n(p)$ is Hall-effect measurements. The Hall coefficient R^H, measured directly on a long thin slab in a standard crossed electric and magnetic field configuration, is retrieved by

$$R^H = 10^{-8}\frac{V_H d}{IB}\,, \tag{21.10}$$

where V_H is the Hall voltage (Volts), I is the current (Amps), d is the sample thickness (cm) in the z-direction, and B is the magnetic field strength (Gauss) applied in this direction. There are two limiting cases. One, the high-field regime is defined by $qB\tau/mc \gg 1$, where m and τ are the appropriate mass and relaxation-time parameters, respectively. In this case

$$\begin{aligned} R_e^H(\infty) &= -\frac{1}{qn}\,, \\ R_h^H(\infty) &= \frac{1}{qp}\,. \end{aligned} \tag{21.11}$$

The other, low-field, regime holds with the opposite inequality; in this regime

$$\begin{aligned} R_e^H(0) &= -\frac{r_e}{qn}\,, \\ R_h^H(0) &= \frac{r_h}{qp}\,, \end{aligned} \tag{21.12}$$

where the constant of proportionality $r_{e(h)}$, called the electron (hole) Hall factor, depends on the details of the scattering process and band structure. Thus the majority-carrier concentration is determined directly from $R^H_{e(h)}$ using a high-field Hall measurement. For typical laboratory magnetic fields, this regime is attainable only with extremely high mobility and low effective mass, which excludes moderately and heavily doped Si, for which very high magnetic fields are required. In some cases the Hall factor is quite close to unity, e.g. $r_e = 3\pi/8$ for the phonon scattering in the isotropic and parabolic (standard) band.

The electrical properties are fully described by the drift-diffusion relation for the electron (hole) current density $j_{e(h)}$

$$\begin{aligned} j_e &= -qn\boldsymbol{v}_{de} + qD_e\nabla n\,, \\ j_h &= qp\boldsymbol{v}_{dh} - qD_h\nabla p\,, \end{aligned} \tag{21.13}$$

where $\boldsymbol{v}_{de} = -\mu_e E$ ($\boldsymbol{v}_{dh} = \mu_h E$) is the drift velocity, $\mu_{e(h)}$ is the drift mobility, E is the electric field strength, and $D_{e(h)}$ is the diffusion coefficient; in general, $\mu_{e(h)}$ and $D_{e(h)}$ depend on E. In the homogeneous case (21.13) converts into the material equation $j_{e(h)} = \sigma_{e(h)}E$, where $\sigma_{e(h)} = qn\mu_{e(h)}$ is the electron (hole) conductivity; the total conductivity equals $\sigma = \sigma_e + \sigma_h$. In the weak-field DC (Ohm) and alternating current (AC: microwave or light, except for intense laser, irradiation) regimes, $D_{e(h)}$ is proportional to $\mu_{e(h)}$ being both constant versus E, depending on the radiation frequency ω.

Combining the high-induction Hall and Ohm resistivity ($\rho = \sigma^{-1}$) measurements one obtains the drift mobility

$$\mu_{e(h)} = R^H_{e(h)}(\infty)\sigma\,. \tag{21.14}$$

Replacing $R_e^H(\infty)$ by $R_e^H(0)$ in the right-hand side of (21.14), one arrives at the so-called Hall mobility

$$\mu^H_{e(h)} = R^H_{e(h)}(0)\sigma = r_{e(h)}\mu_{e(h)}\,, \tag{21.15}$$

which never equals the drift mobility, although it may be fairly close to it in the cases mentioned above. In general, to extract $n(p)$ from $R_e^H(0)$, the calculation of the $r_{e(h)}$ factor is completed. Magnetoresistance (MR), i.e. ρ versus B measurement, is an important experimental tool as well. Another established method is the Haynes–Shockley experiment, which allows one to measure the minority-carrier drift mobility. In high-electric-field conditions, a noise-measurement technique is used. A relatively novel, time-of-flight technique was used in the latest (to our knowledge) mobility and diffusion-coefficient measurements on lightly doped crystalline Si samples, both in the low- and high-field regimes [21.14].

Basic Optical Parameters

The electromagnetic response of homogeneous nonmagnetic material is governed by the dielectric constant tensor ε, which connects the electric displacement vector $\boldsymbol{D}$ inside the material to $\boldsymbol{E}$ through the material equation $\boldsymbol{D} = \varepsilon E$. For cubic crystals, such as Si, ε is a scalar. An effective-medium homogeneous dielectric constant may be attributed to inhomogeneous and composite materials if the nonhomogeneity feature size is smaller than the radiation wavelength $\lambda = 2\pi c/\omega$. Actually, ε characterizes the material's bulk and therefore loses its sense in nanoscale structures (superlattices, quantum wells etc). The dependence $\varepsilon(\omega)$ expresses the optical dispersion in the material. The dielectric constant is usually represented via its real and imaginary parts: $\varepsilon = \varepsilon_1 + i\varepsilon_2$ ($\varepsilon_2 \geq 0$), connected to each other by the Kramers–Kronig relation (KKR)

$$\varepsilon_1(\omega) = 1 + \frac{2}{\pi}\int_0^\infty \frac{\Omega}{\Omega^2 - \omega^2}\varepsilon_2(\Omega)\mathrm{d}\Omega \,. \qquad (21.16)$$

At low frequency (radio, microwave), in the absence of magnetic fields, $\varepsilon_1 \approx \varepsilon(0)$ and ε_2, which is responsible for dielectric loss, is small. At optical wavelengths, from far-IR to soft X-rays, the basic quantity is the complex refractive index $\sqrt{\varepsilon} = n + ik$. The real refractive index n, which is responsible for wave propagation properties, and the extinction index k, responsible for the field attenuation, are referred to as *optical constants*. They are related to the dielectric constant via:

$$\begin{aligned}
\varepsilon_1 &= n^2 - k^2 \,, \\
\varepsilon_2 &= 2nk \,, \\
n &= \sqrt{\frac{\left(\varepsilon_1^2 + \varepsilon_2^2\right)^{1/2} + \varepsilon_1}{2}} \,, \\
k &= \sqrt{\frac{\left(\varepsilon_1^2 + \varepsilon_2^2\right)^{1/2} - \varepsilon_1}{2}} \,.
\end{aligned} \qquad (21.17)$$

21.1.4 Theory of Electrical and Optical Properties

Boltzmann-Equation Approach

The response of carriers in a band to perturbations away from the thermal–equilibrium state, such as applied electric and magnetic fields or impinging electromagnetic radiation, is described by the deviation of the carrier distribution function $f_s(\boldsymbol{k}, \boldsymbol{r}, t)$ from the equilibrium Fermi–Dirac distribution $f_0[E_s(\boldsymbol{k})]$. The current density equals $\boldsymbol{j}_s = q\int \boldsymbol{v}_s(\boldsymbol{k}) f_s(\boldsymbol{k}, r, t)\mathrm{d}\boldsymbol{k}$, where $\boldsymbol{v}_s(\boldsymbol{k}) = \frac{\partial E_s(\boldsymbol{k})}{\hbar\partial \boldsymbol{k}}$ is the microscopic carrier velocity and the integration is performed over the BZ. The process that balances the external perturbations is scattering of carriers by lattice vibrations (phonons), impurities and other carriers. Impurity scattering dominates transport at low temperatures and remains important at room temperature for moderate and high doping levels, although carrier–carrier scattering also becomes appreciable. Under appropriate conditions, one being that $\hbar\omega \ll \bar{E}$ (where $\bar{E}$ is the average carrier kinetic energy), $f_s(\boldsymbol{k}, \boldsymbol{r}, t)$ satisfies the quasi-classical Boltzmann kinetic equation. In the opposite, quantum, range, radiation influences the scattering process. Generalized kinetic equations, which interpolate between the quasi-classical and quantum regimes, have also been derived [21.34].

There exist various methods of solving the quasi-classical Boltzmann equation. The relaxation-time method, variational method [21.35–37] for low electric fields, and displaced–Maxwell–distribution approximation [21.38] for high electric fields, were used in early studies. In the last three decades the Monte Carlo technique [21.39], which overcomes limitations inherent to these theories and allows one to calculate subtle details of the carrier distribution, has been applied to various semiconductors, including crystalline Si [21.14]. If $\hbar\omega \ll \bar{E}$, the kinetic and optical characteristics are calculated well using transition probabilities between carrier states, with the radiation quantum absorbed or emitted [21.40]. The most problematic is the interme-

Table 21.4 Parameters of the phonon modes in crystalline Si

Mode	Energy (K)				Sound velocity
LO	760	700–735[a]	560	580	
TO	760	–	630–690[a]	680	
LA	0	240–260	500–510[a]	580	8.99×10^5 cm/s
TA	0	140–160	210–260	220	5.39×10^5 cm/s
q	Γ	Δ	S	X	

[a] [21.19]